E-157: A 1.4 Meter–long Plasma Wakefield Acceleration Experiment Using a 30GeV Electron Beam from the Stanford Linear Accelerator Center Linac[+]

M. J. Hogan, R. Assmann[*], F.-J. Decker, R. Iverson, P. Raimondi, S. Rokni, R.H. Siemann,

D. Walz, D. Whittum

Stanford Linear Accelerator Center, Stanford University, Stanford CA 94309

B. Blue, C. E. Clayton, E. Dodd, R. Hemker, C. Joshi, K. A. Marsh, W. B. Mori, S. Wang

University of California Los Angeles, Los Angeles CA 90095

T. Katsouleas, S. Lee, P. Muggli

University of Southern California, Los Angeles CA 90089

P. Catravas, S. Chattopadhyay, E. Esarey, W.P. Leemans

Lawrence Berkeley National Laboratory, Berkeley CA 94720

Abstract

In the E-157 experiment now being conducted at the Stanford Linear Accelerator Center (SLAC), a 30 GeV electron beam of 2×10^{10} electrons in a 0.65mm long bunch is propagated through a 1.4m long Lithium plasma of density up to 2×10^{14} e⁻/cm³. The initial beam density is greater than the plasma density, and the head of the bunch expels the plasma electrons leaving behind a uniform ion channel with transverse focussing fields of up to several thousand Tesla/m. The initial transverse beam size with $\sigma = 50\text{-}100\mu\text{m}$ is larger than the matched size of $5\mu\text{m}$ resulting in up to three beam envelope oscillations within the plasma. Time integrated optical transition radiation (OTR) is used to study the transverse beam profile immediately before and after the plasma to characterize the transverse beam dynamics as a function of plasma density. The head of the bunch deposits energy into plasma wakes, resulting in longitudinal accelerating fields which are witnessed by the tail of the same bunch. A time-resolved Cherenkov imaging system is located in an energy dispersive plane downstream of the plasma. It images the beam onto a streak camera allowing time-resolved measurements of the beam energy spectrum as a function of plasma density. Preliminary experimental data from the first three runs are compared to theory and computer simulations.

Invited talk presented at the
American Physical Society 41st Annual Meeting of the Division of Plasma Physics,
11/15/1999-11/19/1999, Seattle, WA, USA

I. Introduction

Plasma based acceleration schemes [1] utilizing relativistically propagating plasma waves have been under active investigation because of their potential to accelerate charged particles at gradients that are orders of magnitude greater than those currently employed in rf cavities. Specifically, such relativistic plasma waves are excited by using either laser pulses [2] or short electron bunches [3]. Both techniques have shown acceleration of electrons in proof-of-principle experiments [4]. Laser-driven schemes such as the beat-wave accelerator [5], the laser-wake field accelerator [6] and the self-modulated wake field accelerator [7] have accelerated electrons with impressive gradients, much in excess of 1 GeV/m, but over rather small (< 1cm) distances. Consequently, the energy gains have been $\lesssim$ 100 MeV [8]. An electron beam-driven plasma wake field accelerator (PWFA) [9] has accelerated electrons over a longer length (~30 cm) but at a much smaller gradient ($\lesssim$ 50 MeV/m). This is mainly due to the limit on the total charge and length of the drive electron bunch. If plasma-based accelerators are to have any relevance to future high energy colliders it is essential to show high-gradient (>> 100 MeV/m) acceleration over a long distance.

The purpose of the present experiment is to demonstrate acceleration of electrons by plasma wakefield acceleration with gradients in excess of 100 MeV/m over a distance greater than 1m. The experiment called E-157 [10] and described in this paper, is ongoing at the Final Focus Test Beam facility (FFTB) at the Stanford Linear Accelerator Center (SLAC). It is carried out by a multi-institution collaboration involving Lawrence Berkeley National Laboratory (LBNL), SLAC, the University of California at Los Angeles (UCLA) and the University of Southern California (USC).

The experiment uses a high peak-current (>100A), ultra-relativistic (γ>>1) electron bunch from the Stanford Linear Collider to access the so-called under-dense (or "blow-out")

regime of PWFA [11]. In this regime the drive electron-bunch density n_b exceeds that of the plasma density n_p. The plasma electrons are expelled by the space charge of the electron bunch leaving behind an ion channel which, ideally, provides a uniform (along the direction of propagation of the beam), and linear (in the transverse direction) focusing force on the beam. The plasma electrons then rush back into the ion channel to produce "an accelerating bucket" or a longitudinal wake field that can accelerate electrons in the tail of the drive bunch.

For the beam and plasma parameters of our experiment there are several distinct experimental observables in addition to the acceleration of electrons in the tail of the drive bunch. Firstly, for a given length of plasma, the electron beam can undergo several betatron oscillations once the ion channel is established. These produce plasma density dependent oscillations of the electron beam spot size downstream of the plasma. Secondly, during the risetime of the electron bunch, while the ion channel is being formed, different longitudinal parts of the beam will undergo different betatron phase advances. This manifests itself as time dependent focusing of the beam. Third, if there is a head-to-tail offset or tilt to the drive beam, the tail of the beam could oscillate due to the transverse wakefields (or focussing force) and even grow in amplitude due to the hosing instability [12]. Fourth, the bulk of the beam will experience an energy loss when creating the wake. All these effects produce characteristic experimental signatures and have to be quantified in order to clearly isolate the energy gain. This paper describes the current progress towards understanding these related effects.

II. Experimental Apparatus

The bulk of the experimental apparatus is located in the FFTB at the end of the SLAC linac. The principal elements are the Lithium plasma source, integrated mirrors and optical transition radiation (OTR) radiators, and finally an aerogel Cherenkov radiator located in the

energy dispersive region downstream of the plasma. The experiment is shown schematically in Figure 1.

A Electron Beam

The SLAC linac delivers a single electron bunch to the plasma at a rate of either 1 or 10 Hz. The electron beam diagnostics include toroidal current transformers for measuring the beam charge, beam position monitors (BPMs) for measuring beam centroids and charge, wire scanners for measuring the average transverse beam size and its emittance, and dispersive regions for measuring the beam energy spectrum. Typical electron beam and plasma parameters are given in Table I.

Transverse wakefields in the accelerator rf structures can produce head–tail tilts and tail offsets that could lead to false energy gain signatures or no energy gain at all. Thus the set-up of the linac upstream of the plasma is critical [10].

The SLAC linac is currently configured for operation of the positron–electron storage ring PEP-II [13]. Its impact on E-157 is briefly explored. The electron beam is accelerated up to ~ 30GeV in the first two-thirds of the linac for positron production. The rf in the last third of the linac is mostly off. The rf has two principal functions: energy gain and manipulation of the correlated energy spread on the beam to control wakefields – so called BNS damping [14]. No BNS damping in the last third of the linac leads to emittance growth and jitter amplification to unacceptable levels. If the energy spread of the beam is not removed prior to the end of the linac, BNS damping controls the wakefields and beam jitter, but the energy spread leads to chromatic effects in the FFTB. In practice the linac is setup to compromise between these two extremes.

Because of transverse wakefields the beam can have a head–tail offset on the order of tens of microns. Because the tail is offset with respect to the head of the beam, it is offset with respect to the center of the plasma focusing channel (which can be thought of as a quadrupole

focussing in both planes) and receives a wakefield-like deflection. The focussing strength K_r [T/m] for a uniform ion column of density n_0 [cm^{-3}] is approximated by:

$$K_r = 960\pi \frac{n_0}{10^{14}}.$$

For a plasma density of 2 x 10^{14} [cm^{-3}] and focusing gradients on the order of 6,000 T/m, a 10μm offset per longitudinal beam size σ_z can lead to a 2mm deflection in the dispersive plane downstream at the Cherenkov radiator (see Figure 1). This effect can in principle be quantified and subtracted from the energy measurement.

Head–tail effects are dependent on the betatron phase advance through the plasma. When the plasma density-length product is adjusted to correspond to a betatron phase advance equal to an integer multiple of π, the plasma is effectively transparent to the initial transverse beam distribution. When the betatron phase advance is an even multiple of π a particle will exit at its initial transverse position and angle, regardless of its incoming offset with respect to the center of the ion channel. When the betatron phase advance in the plasma is an odd multiple of π the tail will exit at a transverse position and angle opposite its initial position and angle. By adjusting the plasma density to an odd or even multiple of π the tail is either flipped in sign or not changed at all. When operating at this transparency condition, and given the dispersion of 0.085m, a 10μm tail offset would correspond to an apparent energy change of only ~3MeV. Complications to this simple picture are discussed in Section III.

B Plasma Source

Given the drive beam parameters of section A, the plasma wavelength

$$\lambda_p[cm] = \frac{2\pi c}{\omega_p} = 3.34 \times 10^6 n_p^{-\frac{1}{2}}$$

where ω_p is the electron plasma frequency and n_p is the plasma density in cm^{-3}, can be optimized so as to maximize the energy gain of a sufficient number of particles to be detected by the imaging system. There is a tradeoff between maximizing the acceleration gradient and

maximizing the number of particles that get accelerated. The electron bunch length has been measured to be 0.65mm rms. Simulations (discussed in Section III) indicate that the plasma density is optimized when the plasma wavelength is equal to the total bunch ($4\sigma_z$), which gives 2.1×10^{14} e$^-$/cm^{-3}. For the plasma column length in this experiment of 1.4m, operating at the transparency condition requires a density of 1.5×10^{14} e$^-$/cm^{-3}. Simulations performed for this lower plasma density indicate that reducing the plasma density has a minimal effect on the accelerating gradient and are discussed in Section III. The longitudinal density gradient in the plasma must be less than 15% to avoid a de-phasing of more than $\pi/2$ with respect to the accelerating wake.

The neutral lithium vapor that is ionized to become the plasma must have two important characteristics. Firstly, since the impact ionization cross section increases with atomic number Z, it must have a low atomic number to minimize the effect of impact ionization from the 30GeV electrons. Secondly, it must have a low enough ionization potential to be ionized by an available laser system. Lithium (Li), with atomic number 3 and ionization potential of 5.392eV makes a good choice.

A prototype for the photo–ionized Li plasma source has been described in detail elsewhere [15]. A heat pipe oven provides a Li vapor column which is partially ionized by an excimer laser pulse. A stainless steel tube with an inner diameter of 30 mm is fitted with a wire mesh along its inner surface and wrapped on the outside with heater tapes to form a heat pipe. The tube is filled with 30g of solid Li and heated to ~750°C. The heated Li becomes molten and Li vapor expands outwards towards cooling jackets at either end. These jackets are water cooled and work together with a helium (He) buffer gas to confine the Li vapor column and provide sharp (a few cm) Li/He longitudinal boundaries. The cooled Li vapor condenses, and is reheated while migrating back toward the oven center by wicking in the stainless steel wire mesh. The

helium buffer gas is isolated from the beam line ultra-high vacuum by 75μm thick beryllium windows.

An argon–fluorine (ArF) excimer laser provides 8mJ of incident UV (193 nm, 6.45 eV photons) at the entrance to the Li vapor column. It has a rectangular cross section which is de-magnified by a 3:1 telescope to an 8 mm^2 area at the entrance of the plasma, corresponding to a fluence of ~100 mJ/cm^2. The Li has an ionization potential of 5.392eV and an ionization cross section of 1.8 x 10^{-18} cm^{-2} for the 6.45 eV photons [15]. The UV telescope is adjusted to taper the spot size along the vapor column. This counteracts UV absorption by the Li vapor and maintains a constant fluence over the length of the plasma column [15]. Longitudinal and transverse gradients in plasma density, resulting from damage to the optical elements, are being investigated. An approximately 10% ionization fraction ensures that the estimated 0.1% impact ionization of the Li vapor is negligible.

By measuring the incident and transmitted UV energy (E_i and E_t respectively), and using the known ionization cross section of the neutral Li (σ), the line integrated number of neutral Li atoms along a column of length L can be calculated from the exponential attenuation of the photons through single photon ionization:

$$n_0 L = -\frac{1}{\sigma} \ln\left(\frac{E_t}{E_i}\right).$$

The UV energy at the Li-He boundaries can presently not be measured in-situ. Thus, an additional measurement of UV transmission must be made when the oven is cold and no Li vapor is present. In this case any absorbed UV is due to losses in the air or optical elements such as windows, lenses and pellicle mirrors. Further, the reflectivity and transmissivity of the various UV windows, lenses and mirrors changes over time given the hostile environment in which they are operating – high incident laser energy density, X-rays and the electron beam itself. The optical elements degrade, typically over a few hours, and hence the plasma density calculated

from UV absorption becomes more uncertain with integrated run time after the cold oven offset is measured. Mitigating damage to optical elements is an area of vigorous activity in the ongoing experiment.

For the purpose of developing an independent diagnostic for the neutral and plasma density, systematic studies of Cherenkov radiation immediately downstream from the oven at wavelengths near the spectral line of Li neutrals (670 nm) have been performed. Measurement of the Cherenkov cone angle permits direct estimate of the neutral density seen by the electron beam, since the Cherenkov resonance condition depends directly on this quantity [16].

C Optical Transition Radiation Diagnostics

The pellicle mirrors that couple the ionization laser pulse into the plasma (see Figure 1) are 150µm thick fused silica substrates with a multi-layer dielectric high reflectivity (HR) coating for 193nm. By depositing a thin film of aluminum onto the side opposite the HR coating they serve an additional role as sources of OTR at close proximity to the plasma entrance and exit. OTR provides a convenient, non-destructive way to measure the beam transverse profile on a single pulse basis. The electron beam undergoes betatron oscillations as it travels down the length of the plasma. In principle, OTR images downstream of the plasma allow for tuning the plasma density such that the beam envelope undergoes an integer number of oscillations and the plasma can be considered transparent to the transverse dynamics. In practice, fluctuations in laser energy give rise to fluctuations in the plasma density and the downstream OTR serves to monitor these deviations from the ideal.

The validity of OTR as a diagnostic for multi–GeV beams was recently confirmed as part of an E-157 test run at SLAC [17] in which 50 µm spot sizes were resolved, in agreement with independent measurements. Although the radiation peaks at an angle $1/\gamma$, at multi–GeV energies a large fraction of the radiation is in the wings of the distribution and has consequences for the

resolution of an OTR based imaging system. The FWHM of an image of a point source, resolved using OTR, is obtained by integrating the single point function, but can be estimated for an optical system of angular acceptance (θ_a) and wavelength λ [18]:

$$FWHM \cong \frac{1.44\lambda}{\theta_a}$$

OTR from the aluminum coating exits the vacuum through a viewport and is imaged onto a Charge-Coupled Device (CCD) camera by a high–resolution compound lens. The angular acceptance is sufficient for a total resolution of the order of 10µm. The overall resolution, which includes effects from finite pixel size etc, is typically larger, on the order of 20µm. Images from the cooled CCD cameras, with dynamic ranges of 12 and 16 bits, are digitized by computers that tag the images and store them to disk.

D Cherenkov Radiation Diagnostic

As discussed in Section III, the peak accelerating field occurs in the back of the electron bunch. As the accelerating gradient increases within the electron bunch, the number of electrons present to witness the accelerating field is progressively lower. Additionally, the number of accelerated electrons that can be resolved is directly proportional to the number of photons created and transported to the streak camera. Recent measurements at SLAC demonstrated that an aerogel based Cherenkov system delivered a factor of 20 more photons than an OTR based system for similar beam conditions [19]. Measuring the combined effects of the transverse and longitudinal fields as depicted in Figures 2-5, requires measuring the beam energy as a function of time with spatial resolutions of the order of 150 µm (corresponding to an energy resolution of 50MeV) and a temporal resolution of one picosecond, respectively. Since housing the streak camera in the radiation enclosure of the FFTB beamline is undesirable due to the limited access afforded, the aerogel radiator is imaged onto the slit of the streak camera located outside the radiation shielding some 15m away. All reflective optics are used to prevent temporal resolution

degradation due to dispersion in transmissive optical elements. The mirrors are coated with an enhanced aluminum coating that is 90-95% reflective over the bulk of the visible spectrum (400nm–700nm), resulting in an overall transmission efficiency of roughly 25%. Field mirrors allow for a field of view (FOV) of ~7mm. For an electron beam energy of 30 GeV and a dispersion (η) of 0.085m, this corresponds to a total imaged energy spread of up to

$$\Delta E = E\frac{FOV}{\eta} = 2.5GeV.$$

Spatial resolution is of the order of 100μm and temporal resolution (including the contribution from the streak camera entrance slit width) is one picosecond. A beam splitter samples a fraction of the Cherenkov light and provides a time-integrated image of the beam in the transverse plane. Monitoring the transverse size provides an additional diagnostic as well as ensuring that alignment of the electron beam image onto the slit is maintained for both the plasma on and plasma off conditions.

III. Simulations and Predictions

Fully self-consistent particle-in-cell simulations have been performed in two and three-dimensions using the object-oriented parallel code OSIRIS [20]. The code employs a moving window to follow the beam and was run on up to 64 nodes on the Cray T3E at the National Energy Research Scientific Computing Center (NERSC). Simulation results for the energy gain, beam profiles, and betatron behavior are shown in Figures 2-5.

Figure 2 shows the energy gain of the beam in a plasma of density 1.5×10^{14} cm^{-3} in a 2-D simulation with axissymetric cylindrical geometry. Also shown are the number of particles and the maximum particle energy in 0.122ps bins along the z-axis. For this case, the bunch contained 2×10^{10} electrons in a bi-Gaussian round bunch of length σ_z=0.63mm, transverse spot size σ_r=70μm and emittance of 15 mm-mrad. The maximum energy bin had a bin-averaged energy

gain of 250 MeV and the highest energy particle gained 400 MeV. It should be noted that the accelerating gradient scales with the electron bunch charge and inversely with the electron bunch length squared. Future efforts will study the effects of increasing the electron bunch charge by up to a factor of two and/or decreasing the electron bunch length by 30%.

Figures 3 and 4 show images from 3-D simulations of the beam (y vs. z) at the exit of the plasma and again after 12m of free space propagation to the Cherenkov detector (not including energy dispersion from the magnet). In order to simulate head-tail offsets of the type that can occur in the experiment, the beam was initialized with a linear cant in the y-direction of 10μm per σ_z (0.63mm). In Figure 3 the beam is exiting the plasma at z=1.4 meters after three envelope oscillations (see Figure 5), while in Figure 4 it exits after 2.5 envelope oscillations. In the experiment, the spot size measured at the Cherenkov detector is a combination of both the transverse size and the dispersed energy spectrum of the electron beam, adding together in quadrature. The blowup of the beam in Figure 4b illustrates how in the experiment a beam diverging at the plasma exit can dominate the measured beam spot size when compared to the contribution from the energy spectrum. Operating at plasma conditions corresponding to an integer number of envelope oscillations minimizes the beam divergence and the subsequent contribution to the time-resolved energy measurement.

Figure 5 shows the y-centroid and y-spot size of an axial slice 440 microns behind the center of the beam as a function of distance propagated into the plasma (corresponding to the 3-D simulation of Figure 3). We see the regular oscillations of the spot size. The centroid of this slice is initially at y=-7 microns and oscillates approximately about an axis defined by the head of the beam at y=+7 microns. The period of the tail-flipping apparent in Figure 5b is roughly twice the period of the envelope oscillations. Therefor, if the electron beam enters the plasma with a head-to-tail offset or tilt, the tail of the beam will oscillate due to the perpendicular wakefields and could even grow due to the hosing instability [12] [20]. The 3D simulations

shown in Figure 5b indicate that although the plasma density may be such that the bulk of the beam exits the plasma with a phase advance of 3π, the tail is slightly out of phase with the bulk of the beam. Consequently, the tail of the beam can exit the plasma with a significant divergence (160-320µrad), which when propagated 12m downstream to the Cherenkov detector, can lead to tail offsets of several mm (see Figure 3b). Such an offset is of the same order, and convoluted with, offsets due to changes in electron energy (see Section D).

IV. Experimental Data

As mentioned in the introduction, there are several distinct experimental observables in addition to the acceleration of electrons in the tail of the drive bunch. Firstly, for a given length of plasma, the electron beam undergoes betatron oscillations once the ion channel is established. These produce plasma density dependent oscillations of the spot size of the electron beam downstream of the plasma. The transverse focussing forces of the ion column should result in betatron oscillations within the plasma of betatron wavelength (λ_β)

$$\lambda_\beta = \sqrt{2\gamma}\,\lambda_p$$

where γ is the relativistic factor. Figure 6 shows the beam undergoing the first envelope oscillation on the time-integrated Cherenkov detector. The plasma density is varied by changing the relative delay between the ionization laser pulse and the arrival of the electron beam, allowing the plasma to decay due to recombination and diffusion. Ideally, the experiment is conducted at a plasma density corresponding to an integer number of beam envelope oscillations to minimize the contribution of transverse dynamics to the time-resolved energy measurement. In practice, fluctuations in both the ionization laser energy (plasma density) and the incomming electron beam distribution necessitate reducing the data based on information such as the laser energy and beam size downstream of the plasma.

Secondly, during the risetime of the electron bunch, while the ion channel is being formed, different parts of the beam will undergo a different number of envelope oscillations. This will manifest itself as time dependent defocusing and focusing along the electron bunch. For the simulations shown in Figures 3a and 3b, the three envelope oscillations are visible in the head of the bunch. The 1 ps resolution of the streak camera diagnostic only resolves the envelope of these oscillations at the head of the bunch.

Due to variations in electron beam tails and ionization laser pulse energy, the diagnostics show a wide variety of images. Figure 7b shows a time-resolved image of the electron beam at the Cherenkov detector, selected because it illustrates many of the effects predicted by the simulations. Figure 7a is a case with plasma off and Figure 7b is with the plasma turned on. In Figure 8, the images from Figure 7 have been processed to illustrate the time dependent features. The images in Figure 7 have been divided into 1.3ps slices. Each slice is then projected onto the vertical axis and fit to a Gaussian. The central contours show the centroid and rms widths of the individual slices. When the projections are non-Gaussian however, the fits do not take into account particles out in the wings. The additional contours in Figure 8 show the maximum extent of particles registering intensities of 50% and 30% of the maximum respectively.

In the plasma off case the beam is roughly cylindrical with no longitudinal correlation in beam energy. Once the plasma is turned on however, the time-resolved image in Figure 7b, as well as the contours in Figure 8b show many of the qualitative features predicted by the simulations. The head of the beam defocuses to ~ 1.5 times the initial transverse size as the electrons are being blown-out, then pinches back down to nearly it's initial size after the ion channel is formed. Third, in the back of the beam where the accelerating gradient is large, there is a shift of particles in the direction of increasing energy.

To differentiate the effect of the transverse dynamics (deflections of tails) from the longitudinal dynamics (acceleration of tails), two techniques are typically employed. Firstly,

'bumps' are placed into the electron beam orbit upstream of the plasma to manipulate the transverse wakefields and deliberately introduce tails into the beam such that their deflection by the plasma can be studied. Secondly, the plasma density is changed from the nominal operating density which corresponds to three envelope oscillations, to a lower density corresponding to two envelope oscillations. After two oscillations in the plasma, an electron emerges with the same radial position and angle as it enters. After three oscillations, an electron exits the plasma with a radial position and momentum opposite to how it entered. This results in 'tail flipping'. These two techniques are used to understand and minimize the contributions to the energy measurement resulting from transverse kicks. When analyzing candidate images for acceleration, these effects have to be considered and quantified – improving our understanding of tail effects is ongoing.

The head of the bunch deposits energy into plasma wakes, resulting in a longitudinal accelerating field which is then witnessed by the tail of the same bunch. For a beam of 2×10^{10} electrons and a plasma density of 1.5×10^{14} Figure 2 predicts that the core of the beam should de-accelerate by up to 100 MeV as it creates the plasma wake. An energy loss of 100MeV corresponds to a change in the centroid location by -285µm at the Cherenkov detector. In the tail of the bunch, where particles witness the longitudinal wake, electrons gain energies up to 400MeV corresponding to an upward shift of 1.2mm. Quantifying the exact values for energy gain and loss via improved statistics and understanding the contributions from transverse effects is the focus of this ongoing experiment.

V. Conclusions

In the ongoing plasma wakefield acceleration experiment E-157, several characteristics of the transverse and longitudinal dynamics predicted by simulations have been observed. The beam transverse size is not matched to the focusing channel produced by the blowout of the

plasma electrons. This results in a modulation of the transverse size of the electron beam downstream of the plasma as a function of the plasma density. Within the rise time of the electron beam, while the ion channel is being formed, different parts of the beam undergo a different number of envelope oscillations, and manifest as time dependent defocusing and focusing of the front of the beam. Quantifying the energy loss of the core and energy gain of the tail, through an improved understanding of the contributions from the deflection of wakefield tails, is the focus of ongoing efforts.

References

[1] E. Esarey, P. Sprangle, J. Krall *et al* "Overview of Plasma Based Accelerator Cocepts," *IEEE Transactions on Plasma Science*, 24, 252 (1996).

[2] T. Tajima and J. M. Dawson, "Laser electron accelerator," *Phys. Rev. Lett*., 43, 267 (1979). M.N. Rosenbluth and C. S. Liu "Excitation of plasma waves by two laser beams," *Phys. Rev. Lett.* 29, 710 (1972).

[3] P. Chen, J. M. Dawson, R.W. Huff, *et al.* "Acceleartion of electrons by the interaction of a bunched electron beam with a plasma", *Phys. Rev. Lett.* , 54, 693 (1985). R. D. Ruth, A. W. Chao, P. L. Morton, *et al.* "A plasma wakefield accelerator," *Particle Acceleraors,* 17, 171 (1985).

[4] C. E. Clayton, K. A. Marsh, A. Dawson, *et al.*, "Ultrahigh-gradient acceleration of injected electrons by laser-excited relativistic electron plasma waves," *Phys. Rev. Lett.* 70, 37 (1993). J. B. Rosenzweig, D. B. Cline, B. Cole, *et al.* "Experimental observation of plasma wakefield acceleration," *Phys. Rev. Lett.* 61, 98 (1998). F. Amiranoff, D. Bernard, B. Cros, *et al.* "Electron acceleration in Nd-laser plasma beat wave experiments," *Phys. Rev. Lett.* 74, 5220 (1995).

[5] M. Everett, A. Lal, D. Gordon, *et al.* "Trapped electron acceleration by a laser-driven relativistic plasma wave,"*Nature* 368, 527 (1994).

[6] F. Amiranoff, S. Baton, D. Bernard, *et al.* "Observation of laser wakefield acceleration of electrons"*Phys. Rev. Lett.* 81, 995 (1998).

[7] A. Modena, Z. Najmudin, A. E. Dangor, *et al.* , "Electron acceleration from the breaking of plasma waves," *Nature* 337, 606 (1995). K. Nakajima, D. Fisher, T. Kawakubo, *et al.* "Observation of ultrahigh gradient electron acceleration by a self-modulated intense short laser pulse," *Phy. Rev. Lett.* 74, 4428 (1995).

C.I. Moore, A. Ting, K. Krushelnick, *et al.* "Electron trapping in self-modulated laser wakefields by Raman Backscatter," *Phys. Rev. Lett.* 79, 3909 (1997).

R. Wagner, S.-Y. Chen, A. Maksimchuk, *et al.* "Electron acceleration by a laser wakefield in a relativistically self-guided channel," *Phys. Rev. Lett.* 78, 3125 (1997).

[8] D. Gordon, K. C. Tzeng, C. E. Clayton, *et al.*, "Observation of electron energies beyond the dephasing limit from a laser-excited relativistic plasma wave," *Phys. Rev. Lett.* 80, 2133 (1998).

[9] J. B. Rosenzweig, D. B. Cline, B. Cole, *et al.* "Experimental observation of plasma wakefield acceleration," *Phys. Rev. Lett.* 61, 98 (1998).

[10] R. Assmann, P. Chen, F. J. Decker, *et al.* "Proposal for a one GeV plasma wakefield acceleration experiment at SLAC," *Nucl. Inst. Meth. A* 410, 396 (1998).

[11] J. B. Rosenzweig, B. Breizman, T. Katsouleas, *et al.* "Acceleration and focusing of electrons in two-dimensional nonlinear plasma wakefields" *Phys. Rev. A* 44, 6189 (1991).

N. Barov, J. B. Rosenzweig, M.E. Conde, *et al.*, "Observation of plasma wakefield acceleration in the underdense regime," *Phys. Rev. ST-AB* 3, 011301 (2000).

[12] M. Lampe, G. Joyce, S.P. Slinker, *et al.* "Electron Hose Instability Of A Relativistic Electron Beam In An Ion Focusing Channel," *Phys. Fluids B5*, 1888 (1993).

J. Krall and G. Joyce, "Transverse equilibrium and stability of the primary beam in the plasma wake-field accelerator," *Physics of Plasmas*, 2, 1326 (1995).

D. H. Whittum, "Cumulative hose instabilities of a magnetically self-focused slab electron beam," *Phys. Fluids B5*, 12 (1993).

[13] J. T. Seeman, "Comissioning Results of the KEKB and PEP-II B-Factories," *Proceedings 1999 Particle Accelerator Conference*, Institute of Electrical and Electronics Engineers, Piscataway, NJ 1999.

[14] V. E. Balakin, A. V. Novokhatsky, V. P. Smirnov, "VLEPP: Transverse Beam Dynamics", *Proceedings of the 12th International Conference on High Energy Accelerators*, Batavia, IL 1983.

[15] P. Muggli, *et al.*, "Photo-ionized Lithium source for plasma accelerator applications", *Proceedings of the 3rd Annual ICFA Conference on 2nd Generation Plasma Based Accelerators, in IEEE Transactions on Plasma Science*, 1999.

S. DiMaggio, L. Archambault, P. Catravas, *et al.* "Development of One Meter-long Lithium Plasma Source and Excimer Mode Reduction for Plasma Wakefield Applications", *Proceedings 1999 Particle Accelerator Conference*, Institute of Electrical and Electronics Engineers, Piscataway, NJ 1999.

[16] P. Catravas, Private Communication.

[17] P. Catravas, W. P. Leemans, E. Esarey, *et al.* "Beam profile measurement at 30 GeV using optical transition radiation", *Proceedings 1999 Particle Accelerator Conference*, Institute of Electrical and Electronics Engineers, Piscataway, NJ 1999.

[18] V. A. Lebedev, "Diffraction–limited resolution of the optical transition radiation monitor*"*, *Nucl. Instr. And Meth. A* 372, 344 (1996).

M. Castellano and V. A. Verzilov, "Spatial resolution in optical transition beam diagnostics", *Phys. Rev. ST Accel. Beams*, 1, 062801 (1998).

[19] R. Assmann, P. Chen, F.-J. Decker *et al.*, "Progress Towards E-157: A one GeV plasma wakefield acceleration experiment", *Proceedings 1999 Particle Accelerator Conference*, Institute of Electrical and Electronics Engineers, Piscataway, NJ 1999.

[20] R.G.Hemker, F.S.Tsung, V.K.Decyk, *et al.* "Development of a parallel code for modeling plasma based accelerators", *Proceedings 1999 Particle Accelerator Conference*, Institute of Electrical and Electronics Engineers, Piscataway, NJ 1999.

Table I: Nominal electron beam and plasma parameters.

Parameter	Value
Electron Beam	
Number of electrons (N_e)	2 x 10^{10}
Energy (E)	30 GeV
Energy Spread – uncorrelated	0.3%
Energy Spread – correlated	Variable to 1%
Bunch Length (σ_z)	0.65 mm
Horizontal Spot Size (σ_x)	50–100 µm
Vertical Spot Size (σ_y)	50–100 µm
Normalized x Emittance (ε_x)	60 mm-mrad
Normalized y Emittance (ε_y)	8 mm-mrad
Repetition Rate	1 or 10 Hz
Plasma	
Plasma length	1.4 m
Plasma Density [e^-/cm^3]	< 2 x 10^{14}
Fractional Ionization	~10%

Figure 1:The E-157 experiment is shown schematically: a 30GeV electron bunch from the SLAC linac is propagated through a 1.4m long photo-ionized Li plasma of density up to 2 x 10^{14} e^-/cm^3. The bunch exits the plasma and is dispersed by a dipole magnet. A Cherenkov imaging system in the dispersive plane images the beam onto the slit of a streak camera to resolve the beam energy and energy spread as a function of time.

Figure 2: Simulation results predicting the core of the electron bunch should loose up to 125 MeV creating the plasma wake, while particles in the tail should gain an average energy of 275MeV with a maximum energy of 400MeV.

Figures 3a and 3b: Simulations showing an electron bunch of 2 x 10^{10} electrons, with an initial tilt of 10 µm radially per σ_z, at the exit the plasma. The bunch undergoes a total of three envelope oscillations within the 1.4m plasma column of density 1.5 x 10^{14} e^-/cm^3. Figure 3a shows the bunch at the exit of the plasma. Figure 3b shows the same bunch propagated 12m downstream to the Cherenkov detector (not including energy dispersion). With an initial tilt on the bunch, the tail could exit the plasma with enough divergence to cause offsets on the order of a few mm when propagated 12 m downstream to the Cherenkov detector.

Figures 4a and 4b: Simulations showing an electron bunch of 2 x 10^{10} electrons exiting the plasma after undergoing only 2.5 envelope oscillations within the plasma. Figure 4a shows the bunch at the exit of the plasma and Figure 4b shows the same bunch propagated 12 m downstream to the Cherenkov detector (not including dispersion). The beam exits the plasma at a waist with a large divergence that results in the beam blowing up to such an extent that the transverse size and divergence would obscure the energy measurements.

Figures 5a and 5b: Simulations showing the effect of the plasma on a beam that enters the plasma with a vertical tilt of 10µm per σ_z. Although the envelope of this particular tail slice (440µm back from the head) may undergo three oscillations (Figure 5a), the centroid oscillates about the head of the beam at slightly less than half the envelope frequency (Figure5b). Particles in the tail can thus exit the plasma with up to 320µrad of divergence which leads to offsets of the order of a few mm when propagated 12m downstream to the Cherenkov detector

Figure 6: The time-integrated transverse spot size of the electron beam measured at the Cherenkov detector. As the plasma density (estimated from the UV absorption measurement) is increased to a few 10^{13} e^-/cm^3, the beam gradually focuses, blows up, and then refocuses at the detector as the beam undergoes the first envelope oscillation.

Figures 7a and 7b: Selected time resolved images of the electron beam size in the energy dispersive plane for plasma off (Figure 7a) and plasma on (Figure 7b).

Figures 8a and 8b: The Figures 7a and 7b are divided into slices 1.3 ps wide, projected onto the vertical (energy dispersive) axis and then fitted to Gaussians. The position of the peak value as well as the rms width of the individual slices is plotted vs. slice number for both plasma off (Figure 8a) and plasma on (Figure 8b). Additional contours showing the farthest extent of counts having an amplitude of 50% and 30% of the peak value of each individual slice is also plotted.
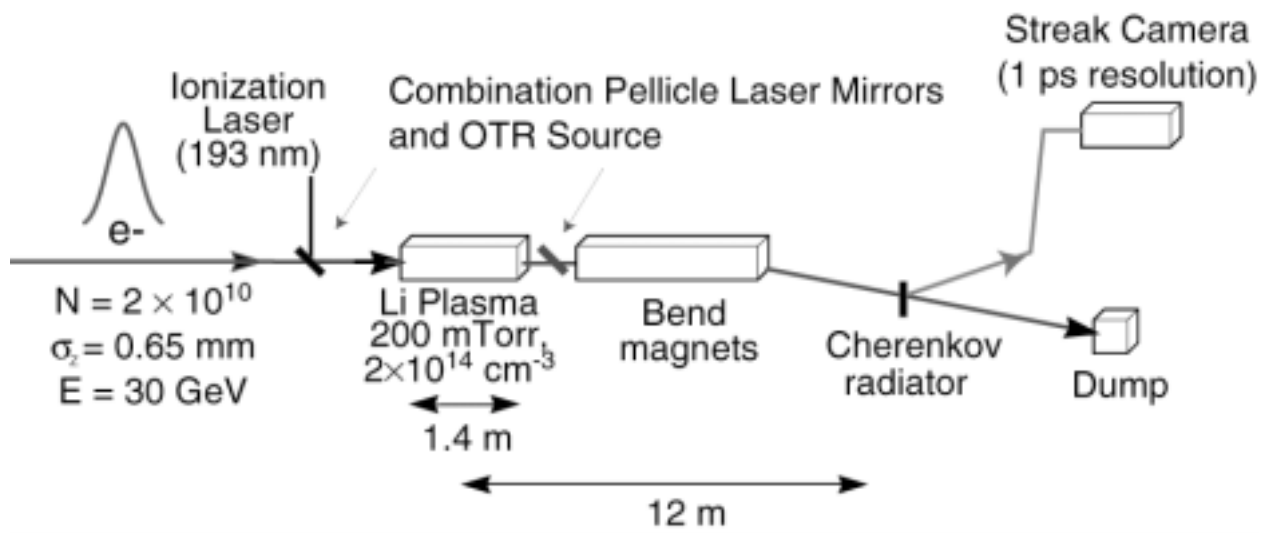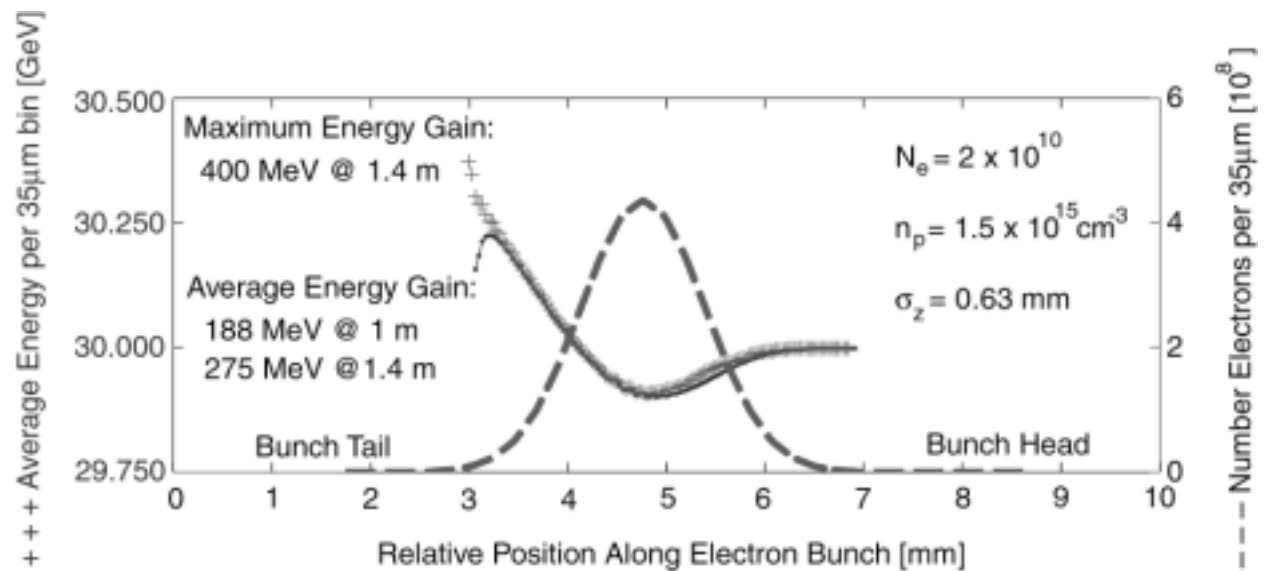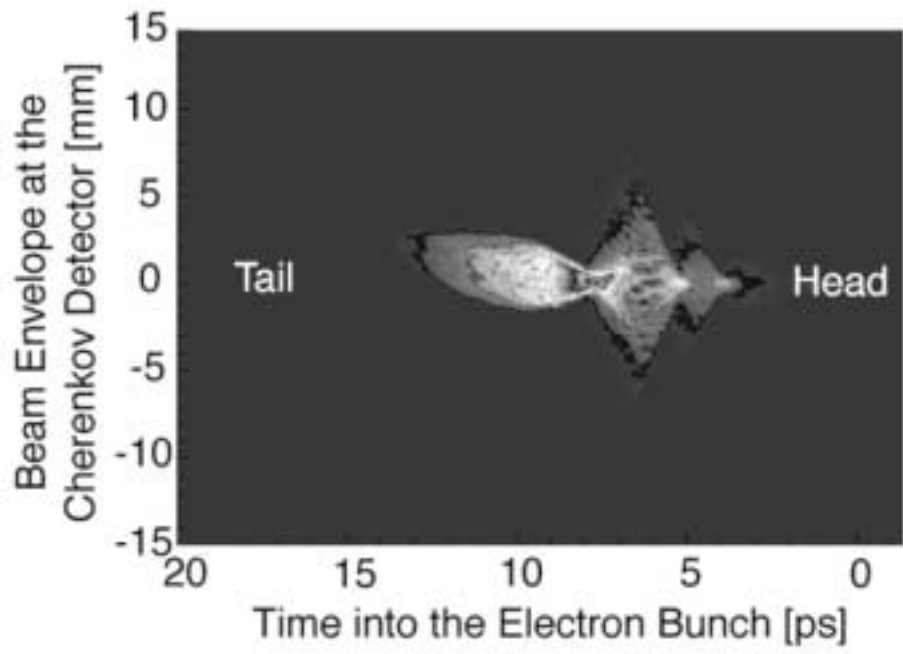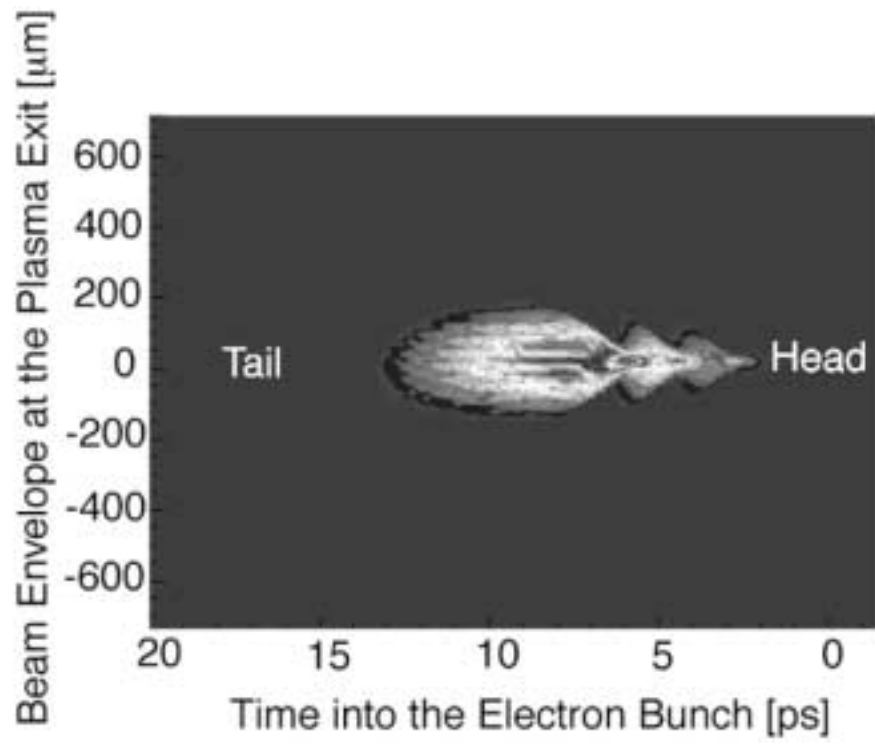
Figure 1

+ + + Average Energy per 35μm bin [GeV]

30.500

30.250

30.000

29.750

Maximum Energy Gain:
400 MeV @ 1.4 m

Average Energy Gain:
188 MeV @ 1 m
275 MeV @ 1.4 m

Bunch Tail

$N_e = 2 \times 10^{10}$

$n_p = 1.5 \times 10^{15} cm^{-3}$

$\sigma_z = 0.63$ mm

Bunch Head

0   1   2   3   4   5   6   7   8   9   10

Relative Position Along Electron Bunch [mm]

6

4

2

0

– – – Number Electrons per 35μm [10^8]
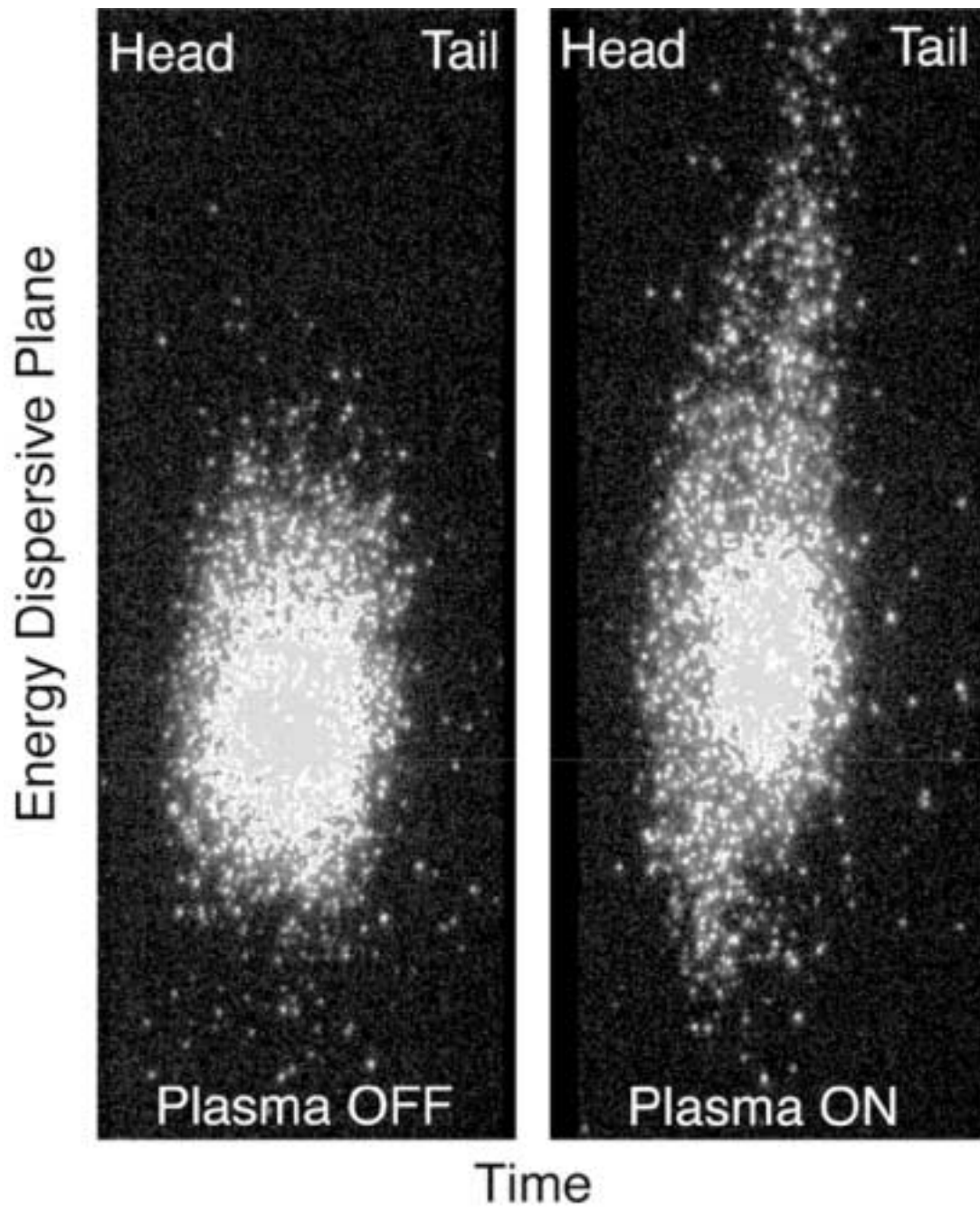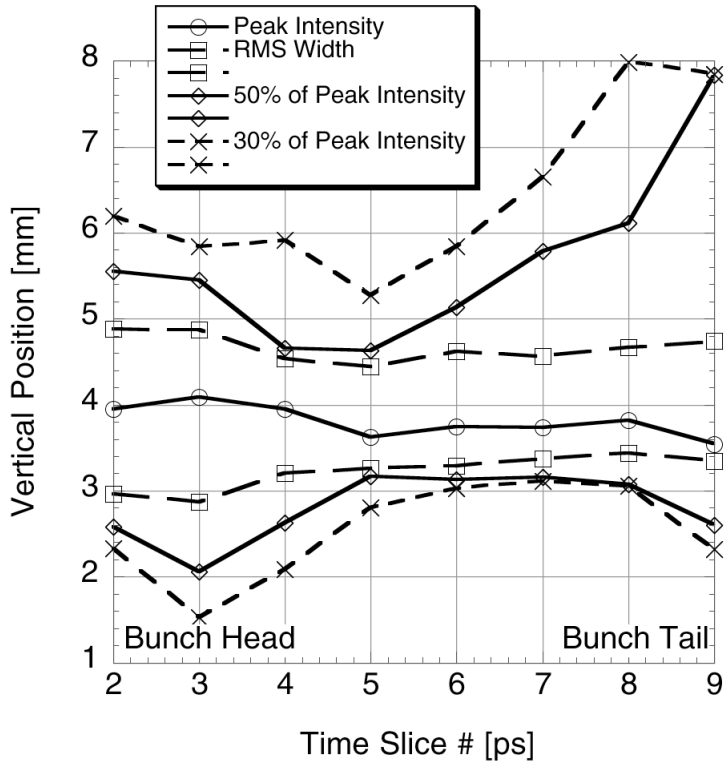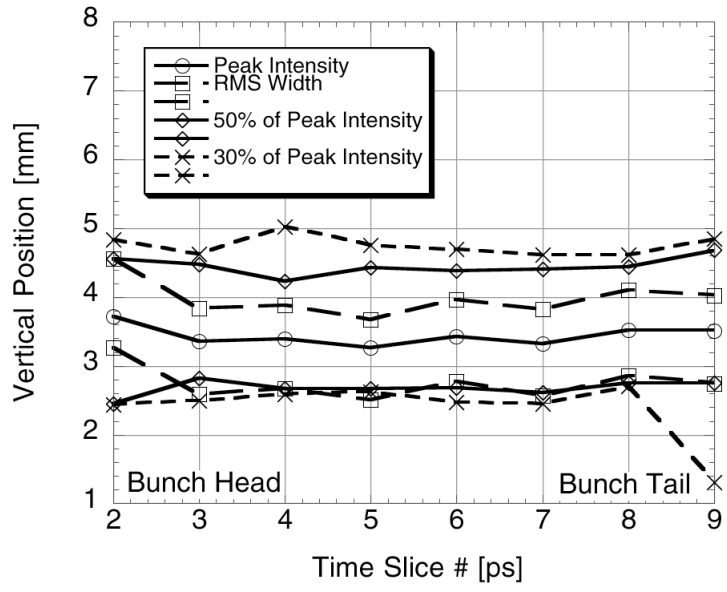
Figure 2

Figures 3a and 3b
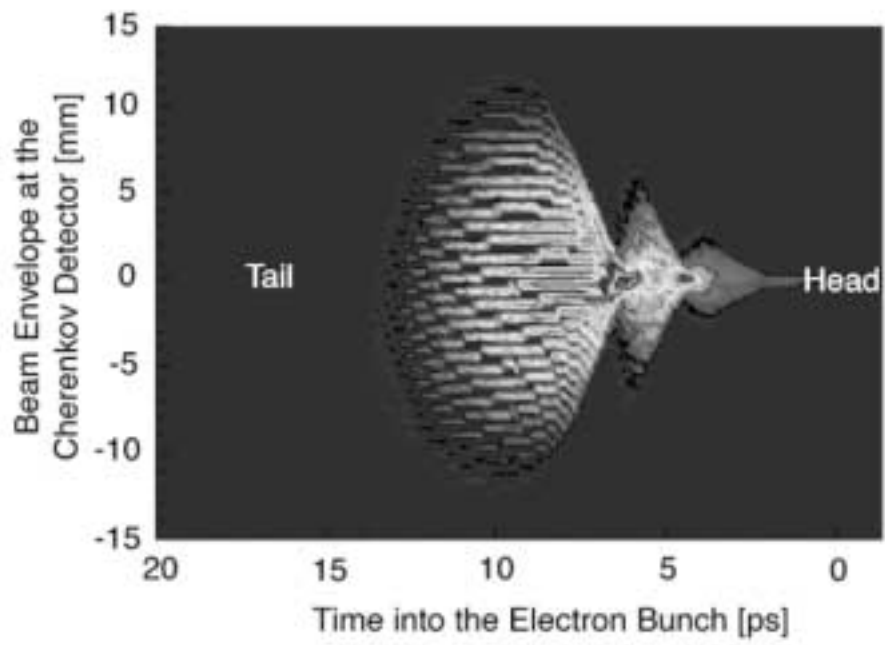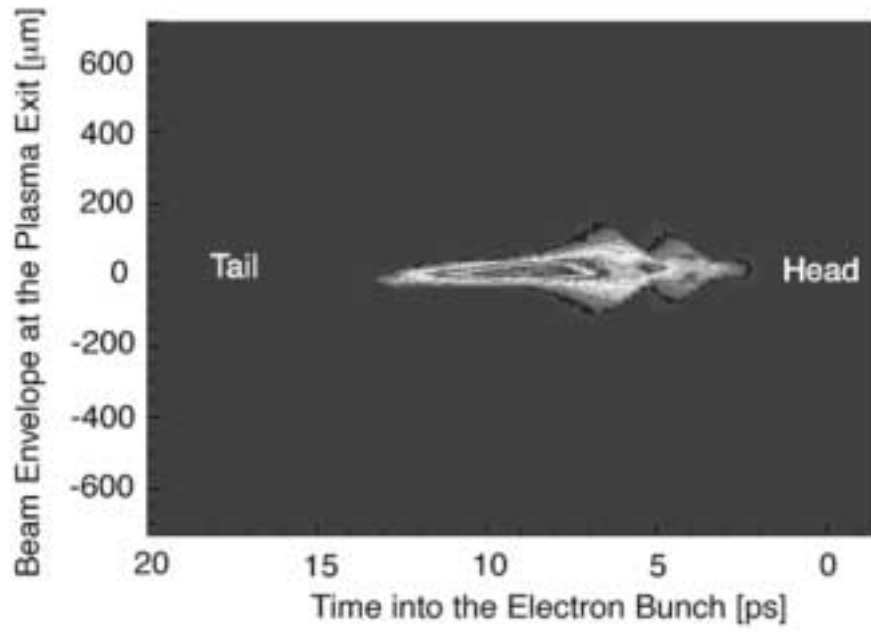
Figures 4a and 4b
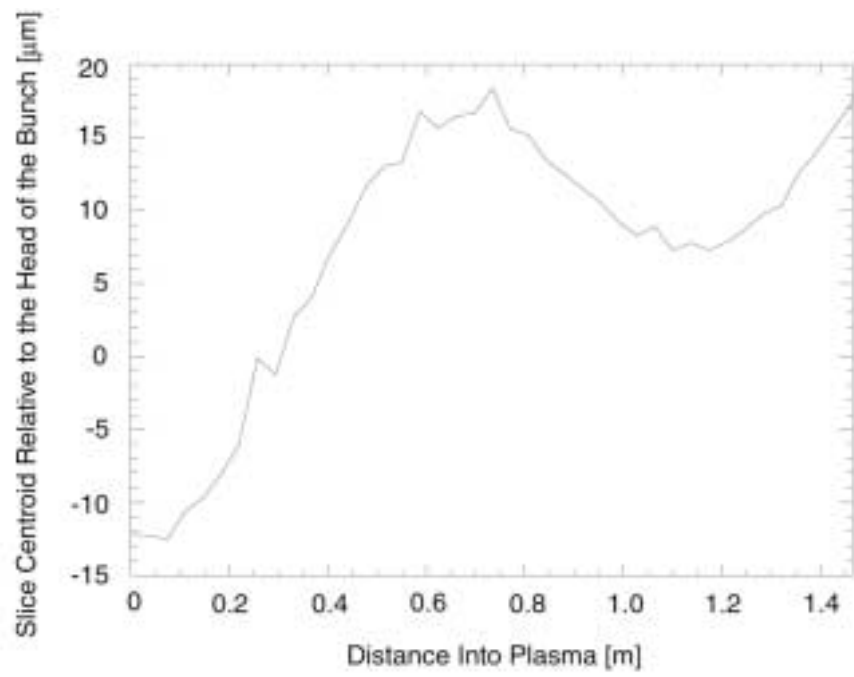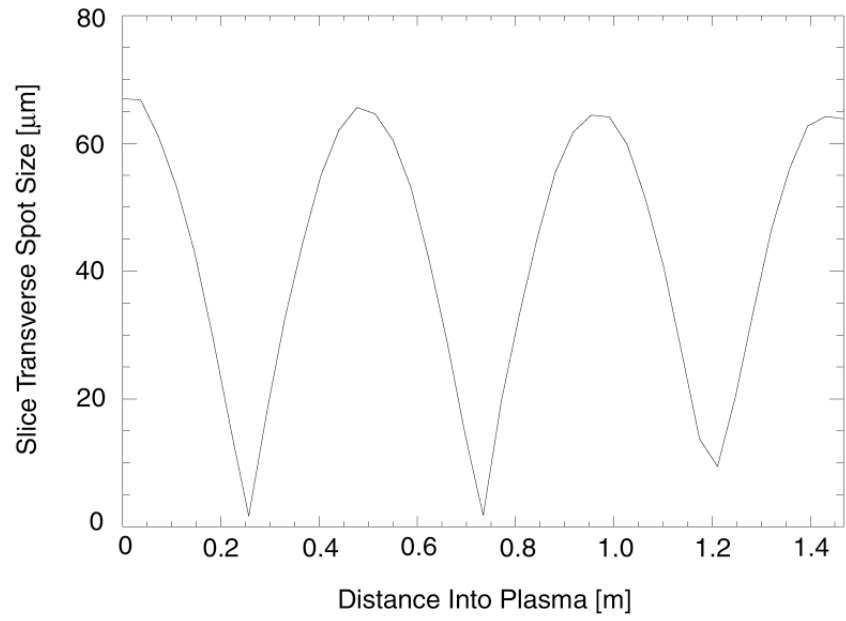
Figures 5a and 5b
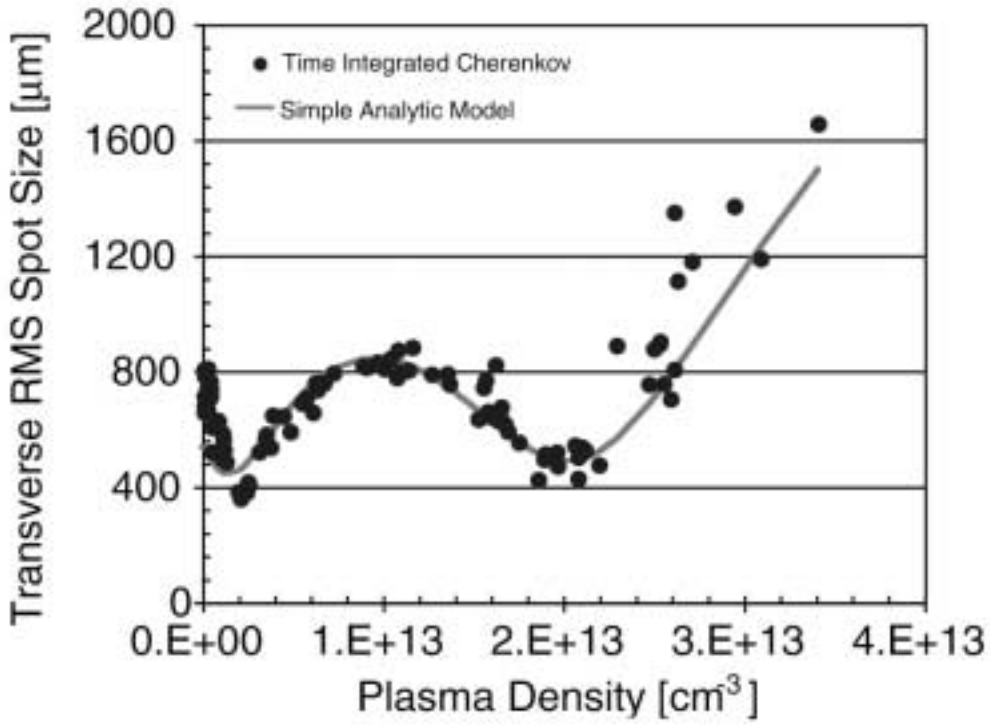
Figure 6

Figures 7a and 7b

Figures 8a and 8b